Engineering Structures 48 (2013) 588–601

Contents lists available at SciVerse ScienceDirect

Engineering Structures

journal homepage: www.elsevier.com/locate/engstruct

Seismic performance of steel beam-to-column moment connections with tapered beam flanges

Cheng-Chih Chen *, Chun-Chou Lin

Department of Civil Engineering, National Chiao Tung University, Taiwan

ARTICLE INFO

Article history:
Received 14 November 2011
Revised 5 October 2012
Accepted 8 October 2012
Available online 27 December 2012

Keywords:
Moment connection
Hysteretic response
Weld access hole

ABSTRACT

This work elucidates experimentally and numerically the behavior of steel beam-to-column moment connections proposed by widening and tapering the portion of beam flanges to increase the ductility and strength of the connection used in moment-resisting frames. Effectiveness of the tapered beam flange and the extent to which geometrical variables of the tapered beam flange affects the connection behavior were examined, based on a parametric study using finite element analysis. Additionally, seven full-scale specimens were tested to clarify their cyclic performance. All of the proposed tapered beam flange specimens, using either the column-tree full welded connection or the web-bolted flange-welded connection, achieved satisfactory ductile behavior by forming a plastic hinge in the beam section away from the column face. Extensive yielding, which occurred in the tapered zone of the beam section, resulted in stable energy dissipation. Based on the parametric study and experimental results, we recommend design parameters and a related procedure for practical design applications.

1. Introduction

Steel special moment frames (SMFs) are extensively used in middle- and high-rise buildings because these highly ductile structural systems can dissipate energy by developing inelastic deformation during strong ground excitation. A typical connection used in SMFs is the web-bolted flange-welded connection, often called "pre-Northridge connection", as shown in Fig. 1. The beam flanges are designed to resist the beam bending moment while the beam web resists the beam shear force. Therefore, the beam flanges are field welded to the column flange by complete joint penetration (CJP) groove welds; meanwhile the beam webs are field bolted to a shear tab. Unfortunately, the 1994 Northridge earthquake caused widespread damage in these steel moment-resisting frames due to the premature failure in the moment connections. The failure was mainly caused by cracking initiated at back-up bars at beam bottom flanges, stress concentration in weld access hole regions, and weld defects at CJP groove weld [1–3]. The seismic performance of the moment connections to avoid such unexpected failure has been extensively studied since the Northridge earthquake. Among the various approaches to improve the seismic performance of moment connections include cover plate, haunch, side-plate, and reduced beam section (RBS) connections [4–8]. Post-Northridge connections have been documented in the literature [9–11].

As an alternative to avoid field welding, a column-tree construction has been used in steel structural systems, especially in Japan and Taiwan [12,13]. Short pieces of a stub beam are fabricated and welded to the column in the shop, forming a column tree. Following the field erection of these tree-like columns, a mid-portion of the link beam is then spliced to the stub beam. This shop welded and field bolted type of the connection is referred to herein as "pre-Kobe connection". Fig. 2 illustrates the column-tree connection details. The defects caused by the field welding are intentionally eliminated because the critical welding of a beam groove weld is done in the shop to improve quality. Nevertheless, the 1995 Hyogoken-Nanbu (Kobe, Japan) earthquake incurred serious failure in these typical pre-Kobe moment connections used for steel column-tree buildings. Nakashima et al. [14] reported premature brittle fractures in the beam-to-column flange groove shop weld which should have been able to improve welding quality. That study also observed limited yielding and plastic deformation developed in the connection.

This work develops a novel scheme of moment connections, capable of increasing the ductility of the connections by widening and tapering portion of beam flanges close to the column. Exactly how the tapered beam flange affects the cyclic behavior of the moment connections is also examined using nonlinear finite element analyses. Moreover, the seismic performance of the tapered beam flange connection is clarified based on an experimental evaluation.

* Corresponding author. Address: Department of Civil Engineering, National Chiao Tung University, Hsinchu 30010, Taiwan. Tel.: +886 3 571 2121x54915; fax: +886 3 572 7109.
E-mail address: chrischen@mail.nctu.edu.tw (C.-C. Chen).

0141-0296/$ - see front matter © 2012 Elsevier Ltd. All rights reserved.
http://dx.doi.org/10.1016/j.engstruct.2012.10.003

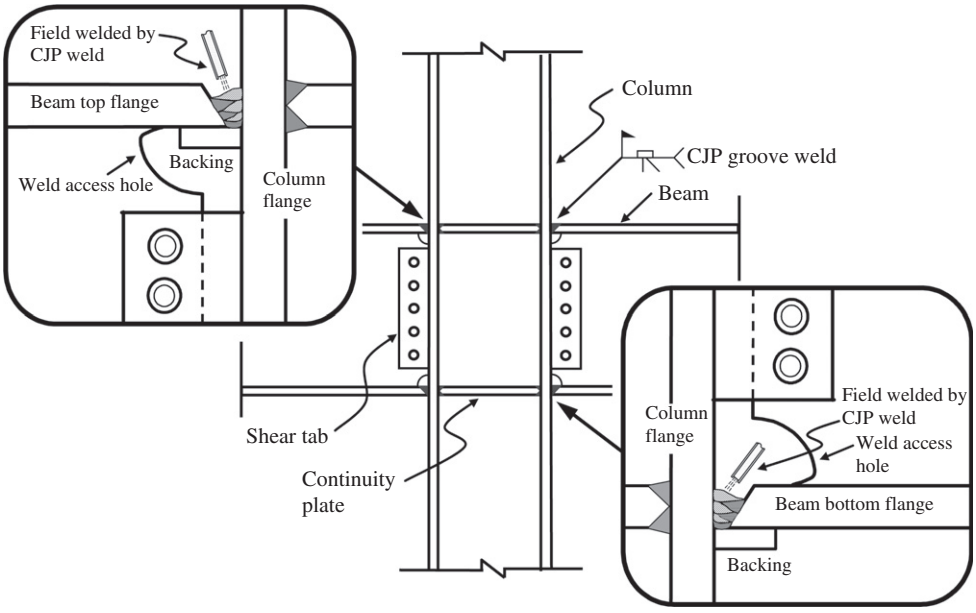

Fig. 1. Typical connection details of web-bolted flange-welded pre-Northridge moment connection.

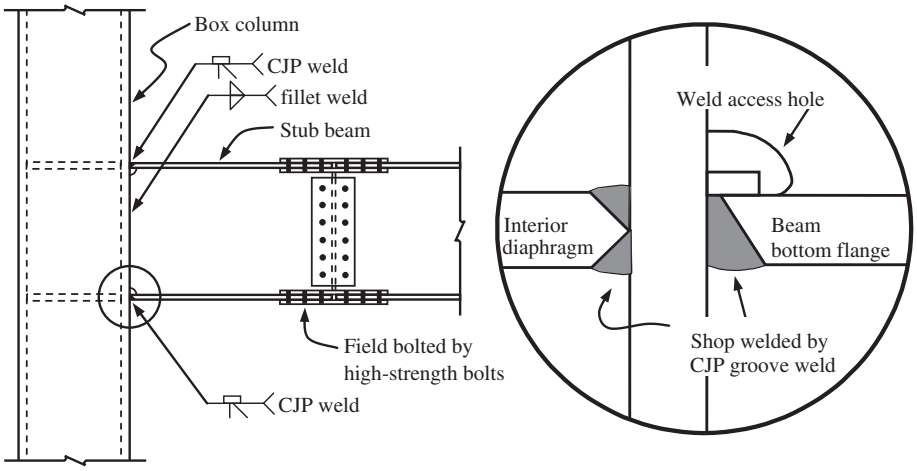

Fig. 2. Typical pre-Kobe column-tree connection.

2. Design concept of tapered beam flange

2.1. Tapered beam flange geometry

Fig. 3 schematically depicts a tapered beam flange moment connection. The design scheme attempts to develop a large plastic zone in the beam to more thoroughly increase the ductile behavior of the moment connection, by tapering a portion of the beam flange along the seismic moment gradient. Two widened plates are designed for the beam flanges rather than welding a flat stiffener on both sides of the beam flange as a wing–plate connection that caused cracking at the tips of the stiffener and subsequent fracture of the beam flange [15,16]. The tapered beam flange comprises a main reinforced part, curved part, tapered zone, and extension. The main reinforced part is used to reduce the demand on the beam-to-column penetration groove weld and ensure the sufficient capacity at the beam-to-column joint. The curved part is designed to provide a smooth transition and the extension provides a splice for a link beam.

The seismic behavior and design of the tapered beam flange connection depend mainly on the flexural capacity of the beam. Fig. 3 also shows the moment gradient of the flexural capacity and seismic moment demand of the beam. By neglecting the effect of gravity loading that is smaller than that of seismic force, the seismic moment demand is the required flexural strength, based on the assumption that a cantilever beam is isolated from the inflection point in the moment frame under the seismic condition. For beams with large spans or significant gravity loading, the moment demand should be adjusted accordingly. According to this figure, an extent of large yielding in the beam is developed simultaneously along the overlapping of two lines of flexural capacity and seismic moment demand.

2.2. Design parameters

According to the design concept of the tapered beam flange connection, two primary variables governing the connection performance are defined as reinforcement ratio β_j and tapered zone

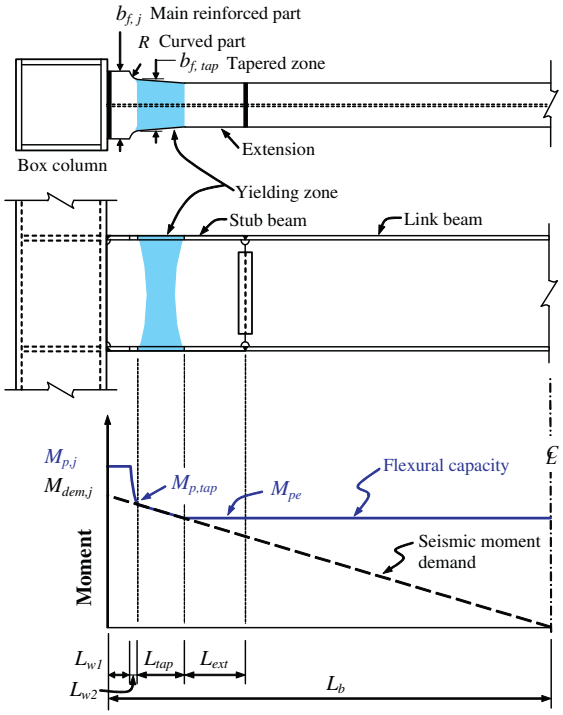

Fig. 3. Geometry and moment gradient of tapered beam flange connection.

length Ltap. While ensuring a sufficient margin of safety at the column face, parameter β_j is defined as the ratio of the flexural capacity, $M_{p,j}$, to the seismic moment demand, $M_{dem,j}$ at the beam-to-column interface.

$$\beta_j = M_{p,j}/M_{dem,j} \quad (1)$$

The other primary parameter L_{tap} is defined to accurately reflect the extent of the yielding zone in a beam. The remaining variables are set a steady value because they slightly influence the behavior of the tapered beam flange connection. The length of the main reinforced part is denoted as L_{w1}. Half a beam flange width $0.5b_f$ is selected for L_{w1} by referring to the design of reduced beam section connection [4] in order to ensure inelastic flexural deformation of the beam moving away from the critical beam-to-column interface. Next, consider the force transfer between the main reinforced part and the tapered zone, in which stress concentration and possible crack initiation are avoided here by using a curved transition L_{w2} of 50 mm. Moreover, the extension L_{ext} is proposed to reduce the stress and the strain demand on the splice joint between the stub beam and the link beam. Half a beam depth ($0.5d_b$) is thus selected here.

3. Experimental investigation

3.1. Design of test specimens

Seven full-scale exterior beam-to-column connections were designed and tested to clarify the cyclic behavior and failure modes of tapered beam flange connections. All specimens have the beam of ASTM A572 Grade 50 H-shaped H700 × 300 × 13 × 24 (dimensions in mm for depth, width, web thickness, and flange thickness, respectively); in addition, the box column is 550 × 550 × 28 × 28 section. Since the cross sectional geometry of the column affects the force transfer between the beam and column as well as connection behavior [17], box columns used in practice are adopted in the specimens. Built-up from four steel plates, box column are widely used in areas of high seismic risk such as Japan and Taiwan. Their popularity is owing to the ability to provide a significant amount of flexural resistance in both axes of the cross section and their use in resisting biaxial bending. To deliver the connection forces more effectively, a special welding process (i.e. electro-slag welding) must be used to weld the interior diaphragm inside the box columns [18]. The size of the beam and column used in the specimen conforms to the design requirements of medium- and low-rise buildings.

Table 1 summarizes the specimen designation. Specimen PK is a conventionally adopted pre-Kobe moment connection used to assess the performance of the welded column-tree connection. Remaining specimens, with tapered beam flange, are grouped into two series: Series W representing the column-tree connection and Series B representing the pre-Northridge web-bolted flange-

Table 1
Summary of test specimens.

Specimen designation	Reinforcement ratio β_j	Tapered zone length L_{tap} ($\times d_b$)	Connection details
PK	–	–	Column-tree connection, beam web welded
W1-L05	1.20	0.5	Column-tree connection, beam web welded
W1-L03	1.20	0.3	
W2-L03	1.10	0.3	
W3-L03	1.05	0.3	
B1-L03	1.20	0.3	Pre-Northridge connection, web-bolted flange-welded
B2-L03	1.10	0.3	

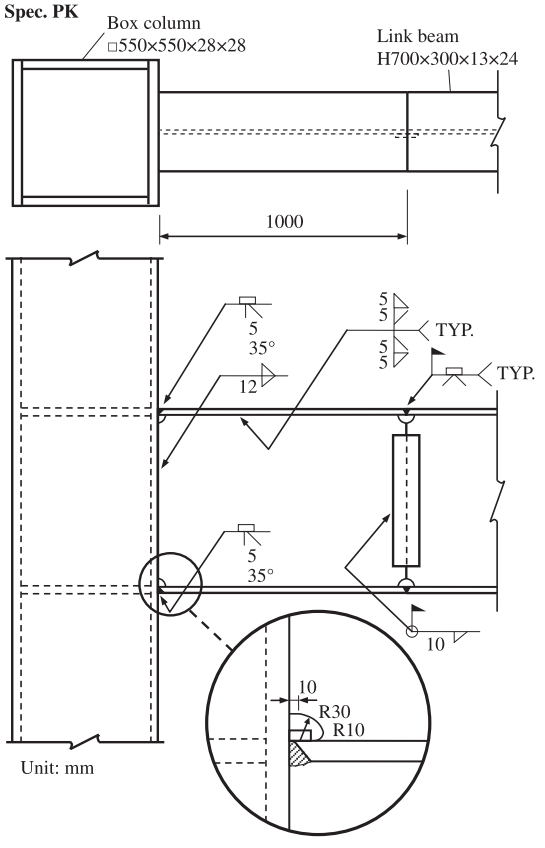

Fig. 4. Connection details of specimen PK.

welded connection. Figs. 4–6 illustrate the connection details for specimens of PK, Series W, and Series B. Specimens of Series W have column-tree connection details. Hence, the root of the beam CJP single bevel groove weld is located on the interior sides of both the top and bottom beam flanges, thus preventing the cracking that initiated from the back-up bar. Erection shear tab is unnecessary for these column-tree connections. Specimens of Series B use the pre-Northridge connection details, and their beams are joined to the column with the web-bolted flange-welded connection.

The proposed connection details for specimens of either Series B or Series W reflect the need for the beam splice. However, the proposed connection details may eliminate concerns over various improved connections. These concerns are such as the decrease of the beam flexural strength in a RBS connection, massive CJP groove welding in a cover plate connection, overhead welding and clear space limitations under the beam in a haunch connection, and prohibition of an orthogonal beam in a side-plate connection. Despite the additional cost for fabricating this built-up tapered beam flange connection, an excellent ductile performance can be guaranteed, as demonstrated in the test results.

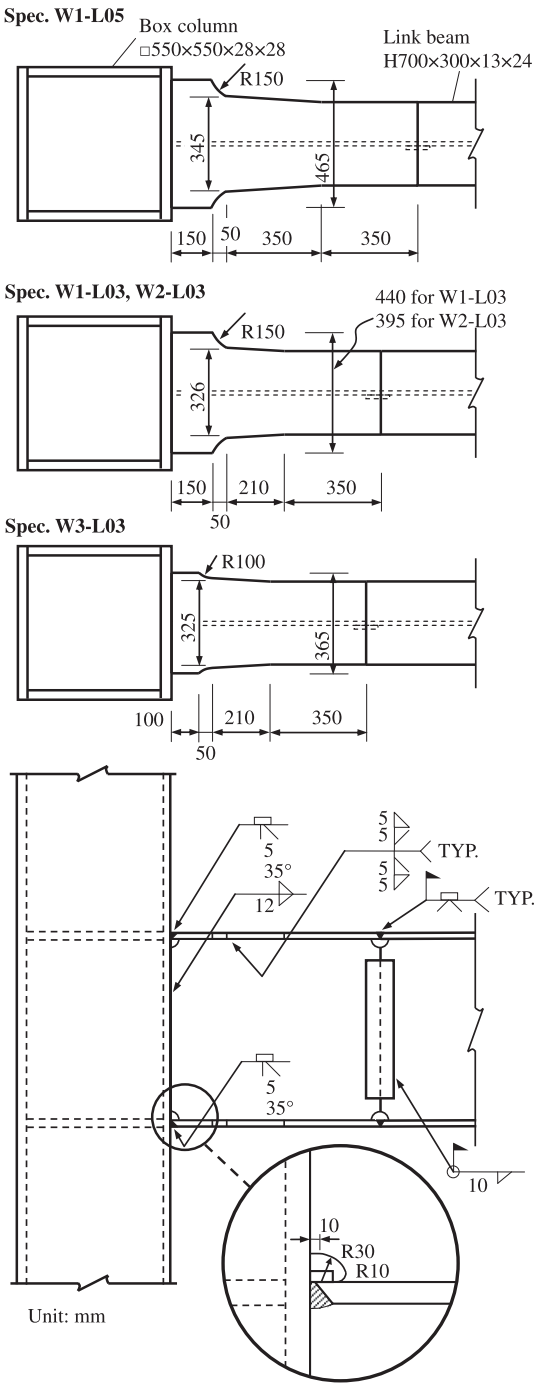

Fig. 5. Connection details of specimens W1-L05, W1-L03, W2-L03 and W3-L03.

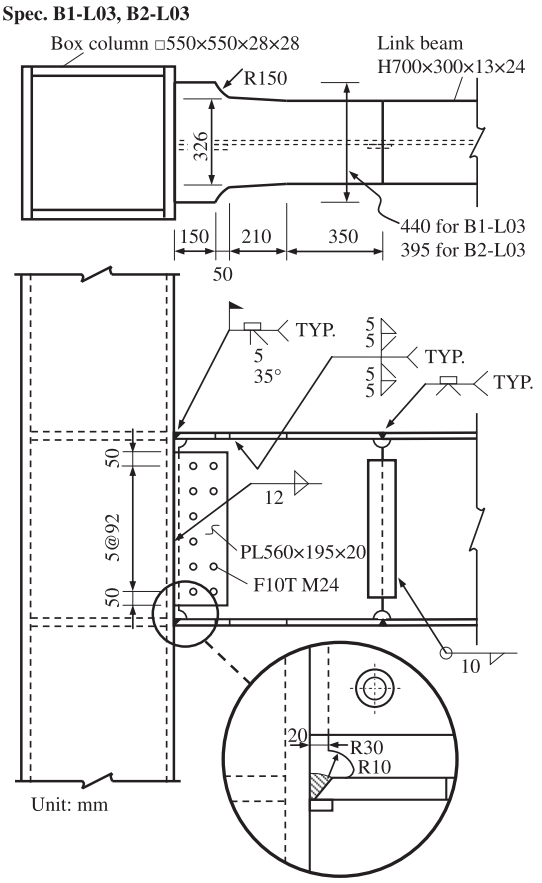

Fig. 6. Connection details of specimens B1-L03 and B2-L03.

Specimens' designation with W1, W2 and W3 refers to the reinforcement ratio β_j of 1.20, 1.10 and 1.05, respectively, resulting in a different width of the main reinforced part. In particular, the smallest width of specimen W3-L03 represents a more critical state. The geometry and size of the tapered flange in the specimens B1-L03 and B2-L03 are the same as those in specimens W1-L03 and W2-L03 except for the beam web attachment. Next, the plastic deformation capacity is evaluated by setting the tapered zone lengths, L_{tap}, to $0.3d_b$ and $0.5d_b$, where d_b denotes the beam depth. Also, the corresponding specimens are designated as "L03" and "L05", respectively.

Table 2 lists the mechanical properties of the steel used for specimens, which were obtained from tensile coupon tests. The ta-

Table 2
Material properties of test specimens.

Member	Coupon location	Yield strength, F_y (MPa)	Tensile strength, F_u (MPa)
Link beam	Beam flange	387	507
	Beam web	429	529
Stub beam	Beam flange	371	511
	Beam web	373	494
Column	Column flange and web	431	578

pered beam flanges were fabricated by a thermal cutting process from a steel plate. The beam CJP groove welds for all specimens were done by the gas metal arc welding process, using an electrode of ER70S-G filler metal.

3.2. Test setup and loading history

Fig. 7 illustrates the test setup which simulated the seismic condition of a connection subassemblage in a moment frame. The cyclic routine was applied with using a hydraulic actuator. According to Fig. 8, a cyclic predetermined loading sequence with increased displacement amplitudes specified in the AISC seismic provisions [19] was used during the tests. The test history began with six cycles of ±0.375, ±0.5, and ±0.75% rad story drift angle. Subsequently, four cycles of ±1% rad story drift angle and two cycles with amplitudes of over ±1.5% rad story drift angle were applied.

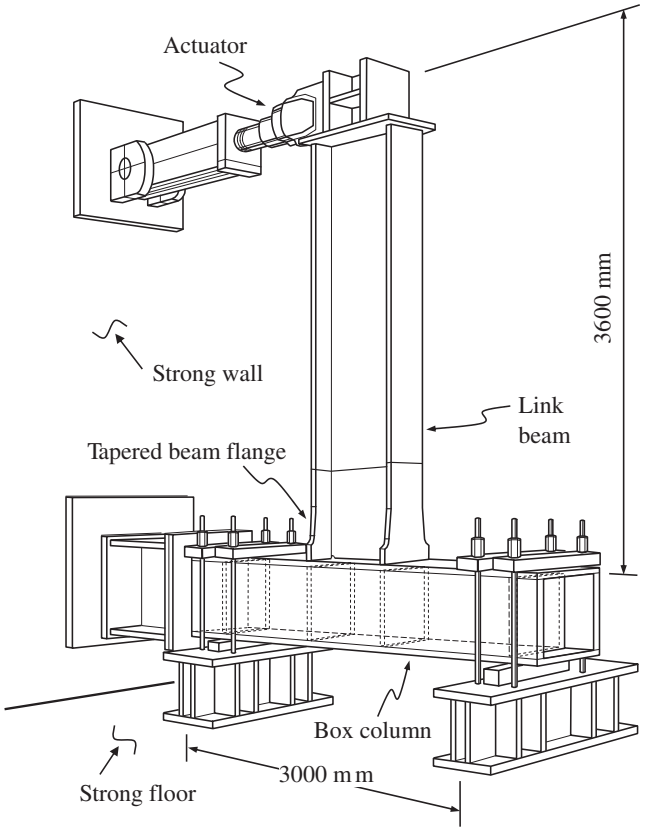

Fig. 7. Overall view of test setup.

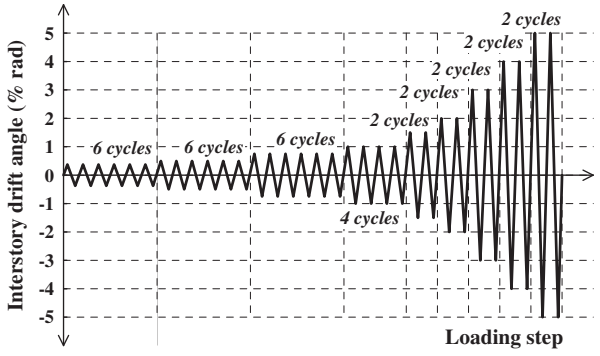

Fig. 8. Loading history.

3.3. Experimental results and discussion

3.3.1. Behavior and failure mode

Table 3 tabulates the test results of the specimens. The cyclic behavior and the failure of the specimens are described briefly as follows.

3.3.1.1. Specimen PK. Specimen PK is a typical pre-Kobe column-tree moment connection. Flaking of the whitewash occurred initially from the sides of the beam flanges near the groove welds during a story drift of 0.5% rad, and significantly concentrated on this location at the following cycles. This finding clearly demonstrates that the beam flange close to the column face develops a high local strain concentration. Afterward, slight cracks were noticed in the fusion zone of the CJP groove weld at the cycles of 3% rad story drift angle. Eventually, specimen PK failed during the negative excursion of the first 4% rad cycle owing to a brittle fracture of the beam top flange, which initiated at the root of WAH, as shown in Fig. 9.

3.3.1.2. Specimens of Series W. Specimens of Series W were designed to contain the column-tree connection. Except for specimen W3-L03, the yielding, plastic hinge formation, and failure mechanisms of all Series W specimens were nearly identical, regardless of the various configurations of the tapered beam flange. During the cycles of 1% rad story drift angle, whitewash was noticed on the beam flanges within the tapered zone and near the CJP groove welds. As demonstrated by the excessive flaking of the whitewash, the overall tapered zone developed a significant amount of inelastic behavior during the cycles of 3% rad story drift angle. Unexpectedly, minor cracks (at both the tips of beam flange groove welds and the root of WAH) were observed during the 3% rad cycles of specimen W3-L03. The sign of cracking apparently revealed that the specimen W3-L03, with reinforcement ratio β_j of 1.05, provides a very small margin of the reinforcement at the beam-to-column interface. Therefore, sustained crack propagation led to fracturing of the beam bottom flange, as shown in Fig. 10, during the positive excursion of the second 4% rad cycle.

Ultimate strength of the specimens was achieved during the cycles of 4% rad story drift angle, which simultaneously accompanied a slight crack initiating at the root of WAH. Excessive local buckling of the beam section, which developed at an approximate range of one-half to three-quarters the beam depth from the column face, gradually deteriorated the strength during the following cycles of 5% rad story drift angle. Fig. 11 displays local buckling of the beam flange and the beam web of specimen W1-L05 at a story drift angle of 5% rad.

3.3.1.3. Specimens of Series B. Specimens of Series B were designed to be constructed as a pre-Northridge connection. Both specimens displayed the same patterns of global behavior with cycles until at 3% rad story drift angle. Flaking of the whitewash was found on the tips of the shear tab near WAH, accompanied with a metallic grating noise caused by slippage between the shear tab and beam web. During 4% rad story drift angle, the ultimate resisting force of specimen B1-L03 was reached while minor cracking was observed at the root of WAH. Simultaneously, the progressive increased buckling of the beam section, stemming from the tapered zone, caused strength degradation during subsequent cycles. Fig. 12 shows the yielding and local buckling patterns of specimens B1-L03 during 5% rad story drift angle. Similar behavior was also observed in specimen B2-L03.

3.3.2. Hysteretic response

Figs. 13–15 plot the hysteretic curves of the beam tip load and beam tip displacement relations as well as the normalized moment

Table 3
Overview of test results.

Specimen	Total story drift rotation (% rad)	Total plastic rotation (% rad)	Beam plastic rotation (% rad)	Description of failure
PK	+4.0 −3.0	+2.6 −1.7	+2.4 −1.4	Fracturing of the beam top flange
W1-L05	+5.0 −5.0	+3.9 −4.0	+3.9 −4.0	Local buckling of beam flanges and web[a]
W1-L03	+5.0 −5.0	+4.0 −4.0	+4.0 −4.0	Local buckling of beam flanges and web[a]
W2-L03	+5.0 −5.0	+4.0 −4.0	+3.9 −3.9	Local buckling of beam flanges and web[a]
W3-L03	+4.0 −5.0	+2.7 −3.9	+2.6 −3.8	Fracturing of the beam bottom flange
B1-L03	+5.0 −5.0	+4.0 −4.0	+3.9 −3.9	Local buckling of beam flanges and web, minor cracking at the root of the weld access hole[a]
B2-L03	+5.0 −5.0	+3.9 −4.0	+3.9 −4.0	Local buckling of beam flanges and web[a]

[a] Test was stopped due to the stroke limitation of the actuator.

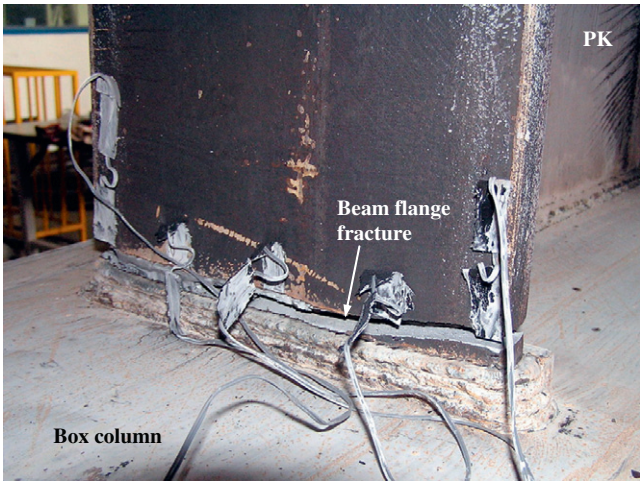

Fig. 9. Fracture of the beam top flange of specimen PK.

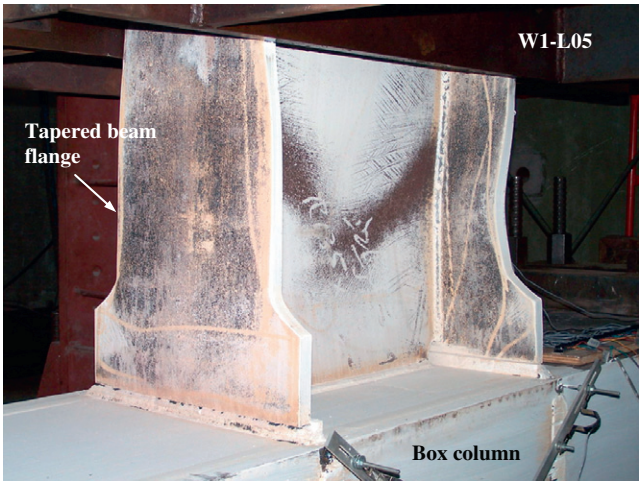

Fig. 11. Plastic hinge formation and local buckling of specimen W1-L05 at 5% rad story drift angle.

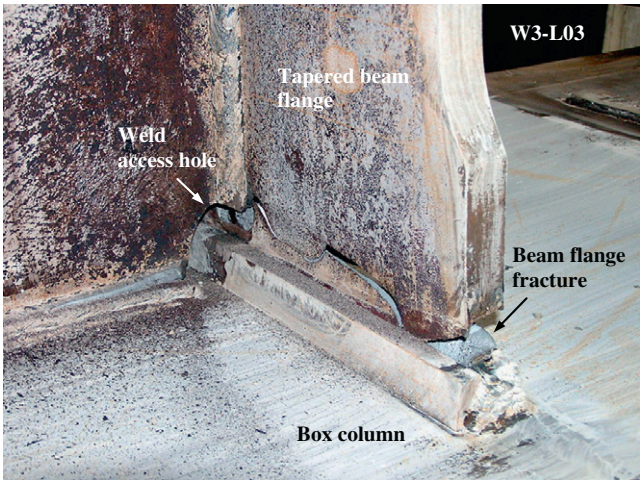

Fig. 10. Fracture of the beam bottom flange of specimen W3-L03 at 4% rad story drift angle.

Fig. 12. Yielding and local buckling of the beam flanges and web of specimen B1-L03 at 5% rad story drift angle.

and story drift angle relations to elucidate the cyclic behavior of the specimens. Herein, the moment calculated to the column face was normalized by the plastic moment capacity of the stub beam based on the measured material strength. The maximum story drift angle of specimen PK was only 3% rad as shown in Fig. 13. Although the ductility of this specimen was higher than that of the pre-Northridge specimens [20], the use of column-tree design practice

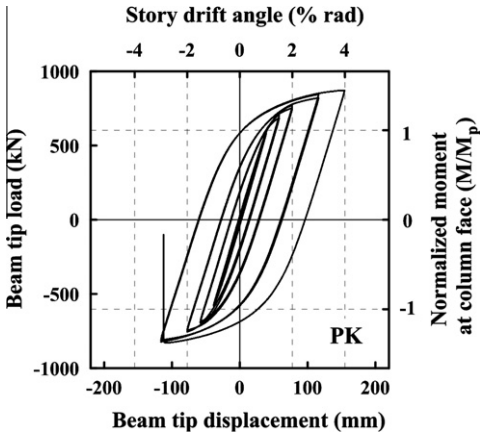

Fig. 13. Hysteretic curve of specimen PK.

in the connection only slightly prevents the beam flange fracture that originated from the WAH region. Fig. 14 shows the hysteretic responses of the Series W specimens which demonstrate stable cyclic behavior. Owing to the local buckling of the beam flange and web, the strength gradually deteriorated in the hysteretic curves. According to Table 3, Series W specimens developed approximately 4% rad of maximum total plastic rotation, which was largely owing to the inelastic deformation of the beam.

The cyclic behavior of the specimens B1-L03 and B2-L03 behaved similar to those column-tree connections – regardless of the different connection details. Fig. 15 displays the hysteretic curves of specimens B1-L03 and B2-L03. Both specimens exhibited reliable inelastic behavior with a maximum story drift angle of 5% rad, absorbing a significant amount of energy. The final failure was owing to prominent local buckling at the beam flanges and web, and was accompanied by gradual deterioration in the flexural strength of the connection. However, the flexural strength still exceeded the plastic flexural strength of the beam. Briefly, the pre-Northridge specimens improved by the tapered beam flange achieved an excellent ductile performance.

3.3.3. Connection moment capacity

Fig. 16 illustrates the ratios of the maximum test moment to calculated plastic moment capacity of the specimens along the longitudinal direction of the beam. These ratios represent the strain-hardening level of the beam section. Notably, the tapered flange provides a flattop level of larger uniform inelastic deformation in the beam away from the column face and stresses the tapered zone of the beam into 1.15 times of the plastic moment capacity. Specimen W1-L03 with β_j of 1.2 gives a more conservative design at the column face than specimen W2-L03 with β_j of 1.1. Consequently, the moment demand at the beam-to-column interface is reduced intentionally by introducing the main reinforced part.

3.3.4. Energy dissipation

Fig. 17 compares energy dissipation levels of the specimens to confirm the effectiveness of the tapered beam flange. Specimen PK dissipated the smallest amount of energy because of a brittle fracture of the beam flange at a story drift angle of 4% rad. Conversely, the successful tapered beam flange connections dissipated an amount of energy approximately 2.4 times that of specimen PK,

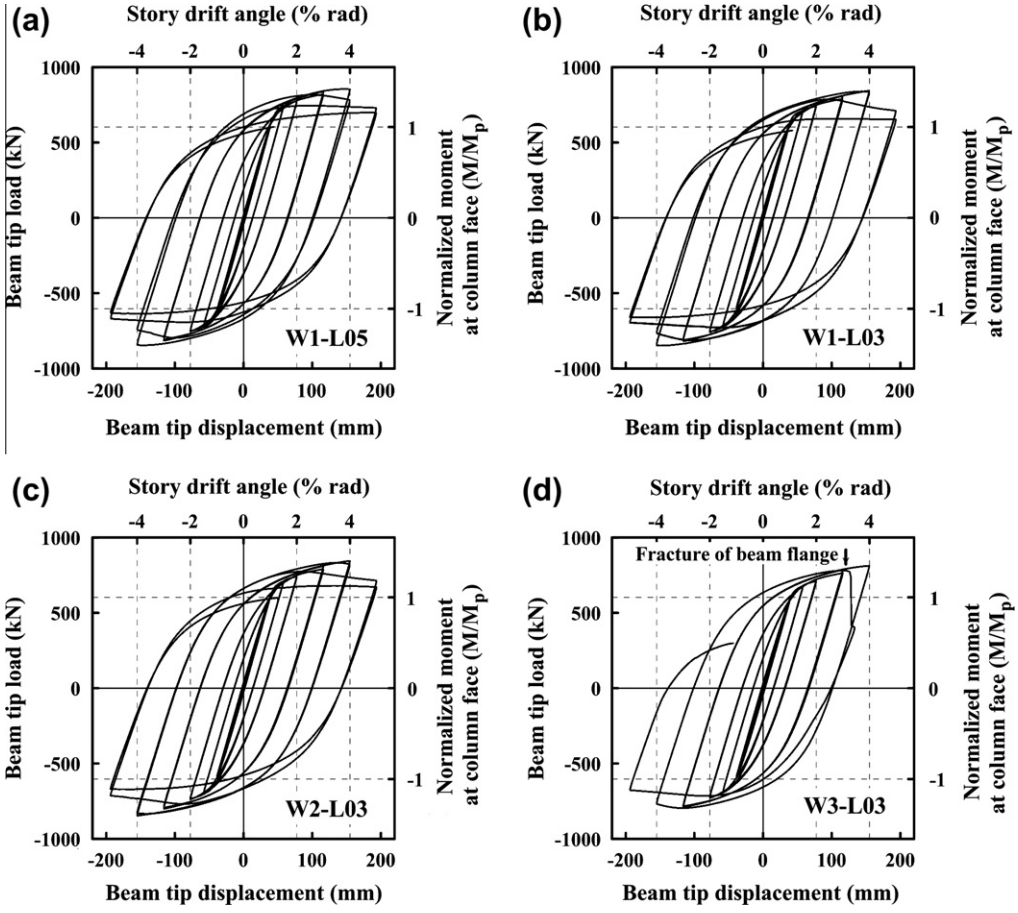

Fig. 14. Hysteretic curves of Series W specimens.

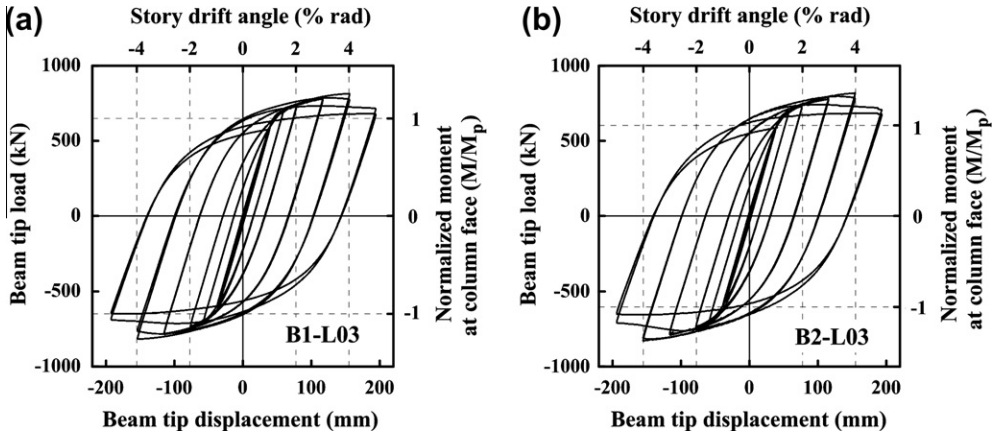

Fig. 15. Hysteretic curves of Series B specimens.

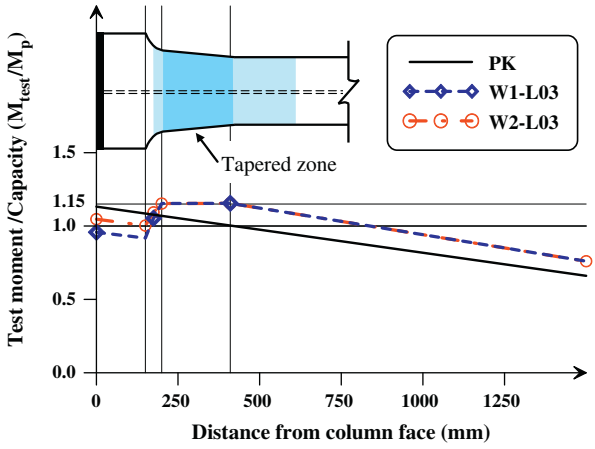

Fig. 16. Ratios of maximum test moment to calculated moment capacity of specimens PK, W1-L03 and W2-L03 along the beam longitudinal direction.

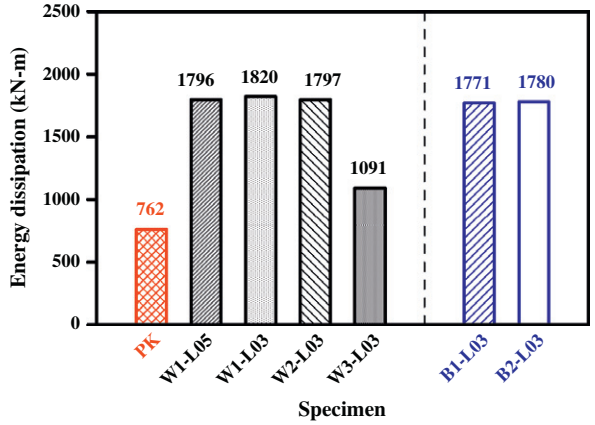

Fig. 17. Comparison of energy dissipation of the specimens.

due to the stable and full hysteretic loops of the specimens. Comparing specimen W1-L03 with W1-L05 reveals a highly similar energy dissipation for these two specimens. Additionally, increasing the length of the tapered beam flange from $0.3d_b$ to $0.5d_b$ slightly affected the connection behavior. Furthermore, although different details of the beam web attachment were used, specimens of Series W and B dissipated a similar amount of energy. This observation clearly indicates that applying the tapered flange can significantly improve the ductility of the specimens, either the column-tree connection or the web-bolted flange-welded connection.

4. Finite element analysis

4.1. Finite element modeling

Based on a general-purpose nonlinear finite element analysis program ANSYS [21], various configurations of the tapered beam flange connection were modeled and analyzed. Exactly how design parameters affect the connection behavior was also more closely examined. The finite element models of the connection subassemblage consisted of three-dimensional structural solid elements with 24 nodal degrees of freedom. Fig. 18 shows the finite element meshes and boundary conditions of the model. Due to the structural symmetry with respect to the mid-plane at the beam web and the column section, only half of the connection subassemblage was modeled to reduce the computational effort. According to Table 4, 13 models were designed for detailed evaluation. An unreinforced connection was modeled to represent the conventional moment connection, while other models with various configurations of the tapered beam flange were designed to clarify the effectiveness of the tapered beam flange on the connection behavior. A control model of the tapered beam flange connection used parameter β_j of 1.2 and L_{tap} of $0.3d_b$. Table 4 also lists the dimensions of the tapered beam flange used in models with the flange width of the main reinforced part ranging from 372 to 530 mm and the stub beam length ranging from 760 to 1110 mm.

For simplification, the stress–strain relations of the structural steel and the weld were simulated based on bilinear isotropic hardening behavior. In particular, a rate-independent plasticity model was used to analyze the inelastic behavior. Moreover, plastification of the models was determined using the von Mises yielding criterion with the associated flow rule. Furthermore, the isotropic hardening rule was used for monotonic analysis, and kinematic hardening behavior of the structural steel was assumed for cyclic analysis.

The potential for cracking was evaluated based on a tendency of stress and strain states at different levels of a story drift angle. According to previous works [22–25], von Mises stress and equivalent plastic strain were used as the indicators of the potential for plasticity in ductile materials. Undoubtedly, a higher PEEQ implied a higher demand for a plastic strain. Meanwhile, the principal stress was normalized by yield strength F_y, while PEEQ divided by the yield strain ε_y defined as the PEEQ index. Two critical sections of the connection, along the beam flange width at the locations of the complete joint penetration groove weld and the root

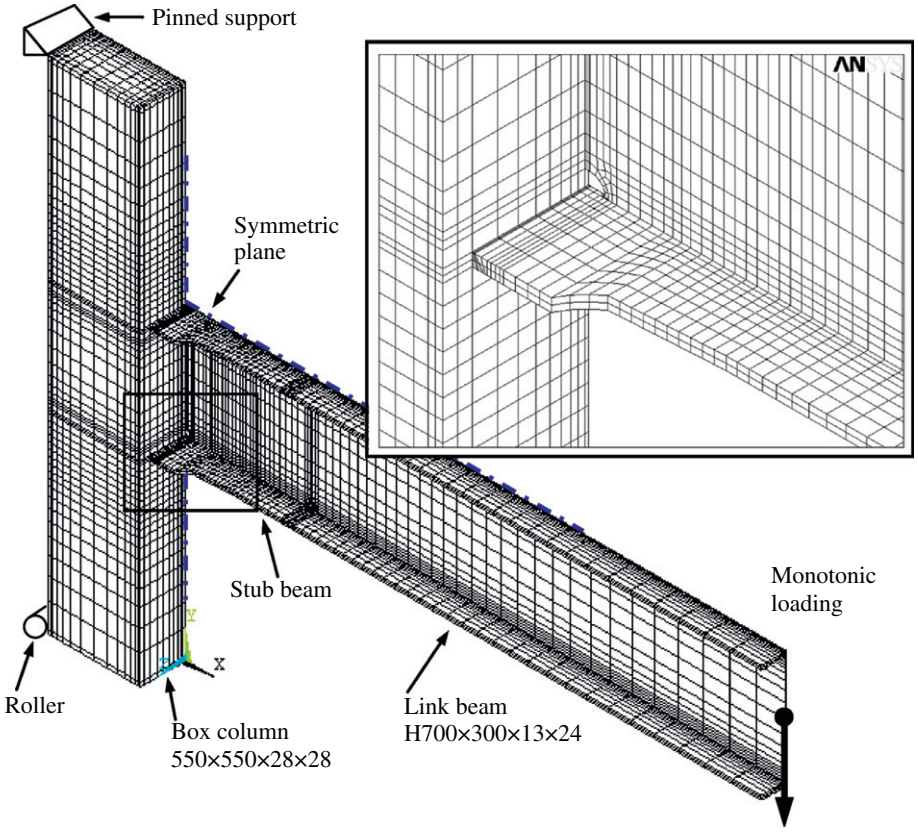

Fig. 18. Finite element modeling.

Table 4
Parameters used in finite element analysis.

Model no.	Parameter		Geometry		Note
	Reinforcement ratio β_j	Tapered zone length L_{tap} ($\times d_b$)	Width of main reinforced part (mm)	Length of stub beam (mm)	
1	1.00	–	300	1000	Unreinforced
2	1.05	0.3	372	760	
3	1.05	0.5	394	900	
4	1.05	0.8	430	1110	
5	1.10	0.3	395	760	
6	1.10	0.5	416	900	
7	1.10	0.8	455	1110	
8	1.20	0.3	440	760	Control model
9	1.20	0.5	463	900	
10	1.20	0.8	505	1110	
11	1.25	0.3	460	760	
12	1.25	0.5	486	900	
13	1.25	0.8	530	1110	

of WAH, were selected to examine the stress and strain statuses based on the fractured locations in the unreinforced moment connections reported in the literature [14,20,26]. Moreover, story drift angles of 0.5% and 4% rad were chosen to investigate the elastic behavior and the plastic deformation state of the connection subassemblage, respectively.

4.2. Verification of finite element model

Fig. 19 shows the experimental and finite element analysis hysteretic curves of the specimen W1-L03. Overall, the load–displacement hysteretic response demonstrates a good correlation between the numerical and the experimental results, except for the deviation due to Bauschinger effect, which was likely caused by simplifying the bilinear strain-hardening behavior of the material.

Next, the local behavior was examined by comparing the numerical strains with test data at various loading steps. Fig. 20 presents both the numerical and measured strains across the beam flange within the tapered zone until 4% rad story drift angle. The elastic response of the test specimen can be simulated precisely, and the inelastic response envelope of the numerical results shows the same trend as test data. The numerical and the experimental results correlated well with each other.

4.3. Analysis results and discussion

4.3.1. Plastification of tapered beam flange connection

Fig. 21 presents the contours of the plastic equivalent strain at a story drift of 4% rad to clarify the spread of the plasticity around the connection. Remarkably, the tapered beam flange connection

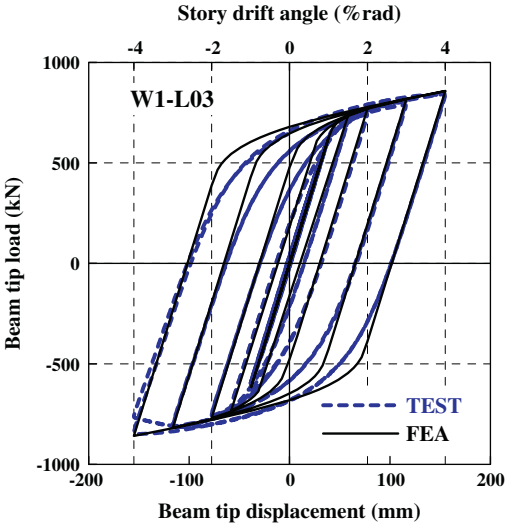

Fig. 19. Comparison of experimental and finite element analysis beam tip load versus beam tip displacement response of specimen W1-L03.

demonstrated extensive plastification and significant yield on the tapered zone, whereas the unreinforced connection developed localized plastic hinge formation close to the beam-to-column interface. Based on the observations shown in this figure, tapering part of the flange plate following the seismic moment demand obviously conduced to the formation of the extensive plasticity in the beam section away from the column face.

4.3.2. Distributions of von Mises stress and equivalent plastic strain

Fig. 22 shows the contours of the von Mises stress and the equivalent plastic strain, with the photographs showing signs of yielding of specimen W1-L03 at 1% and 4% rad story drift angles. Notably, the beam yielded initially at the sides of the beam flange near the beam groove weld during 1% rad story drift angle. At 4% rad story drift angle, the extensive yielding zone strikingly expanded into the entire tapered beam flange. The equivalent plastic strains in the yielding zone are approximately 9.7 times the amount of the yielding strain. An appreciable amount of yielding spread further towards the middle portion of the main reinforced part near WAH. Such highly stressed and strained states could lead to premature cracking at the root of WAH, as evidenced by full-scale tests. Above observations suggest that the moment connection with a tapered beam flange formed extensive yielding and plastification in the beam section away from the beam-to-column interface.

4.3.3. Effect of tapered beam flange on connection behavior

Fig. 23 shows normalized principal stresses at 0.5% rad story drift angle and PEEQ indices at 4% rad story drift angle along the width of the beam flange, at the CJP groove weld and at the root of WAH. Both locations are vulnerable because the localized stress concentration at these two locations initiated cracking, subsequently fracturing the beam flange [2,14,20,26]. Both connections show a high stress concentration at the tips of the groove weld during a story drift angle of 0.5% rad. Such stress flow is attributed mainly to the stiffness of the column web on both sides, as presented in previous analyses [17,27]. Stress concentration was observed at the root of WAH, because of the discontinuous geometry due to WAH. However, when the tapered beam flange

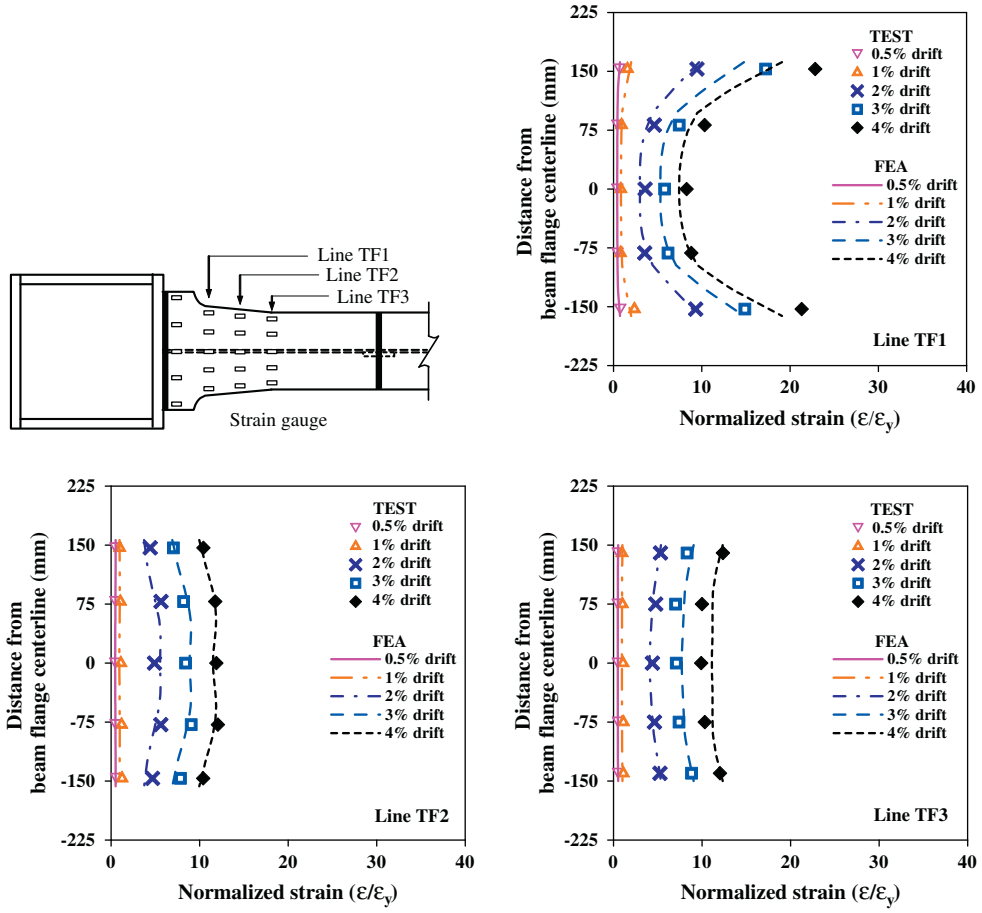

Fig. 20. Longitudinal strain distributions around tapered zone of the beam flange for specimen W1-L03.

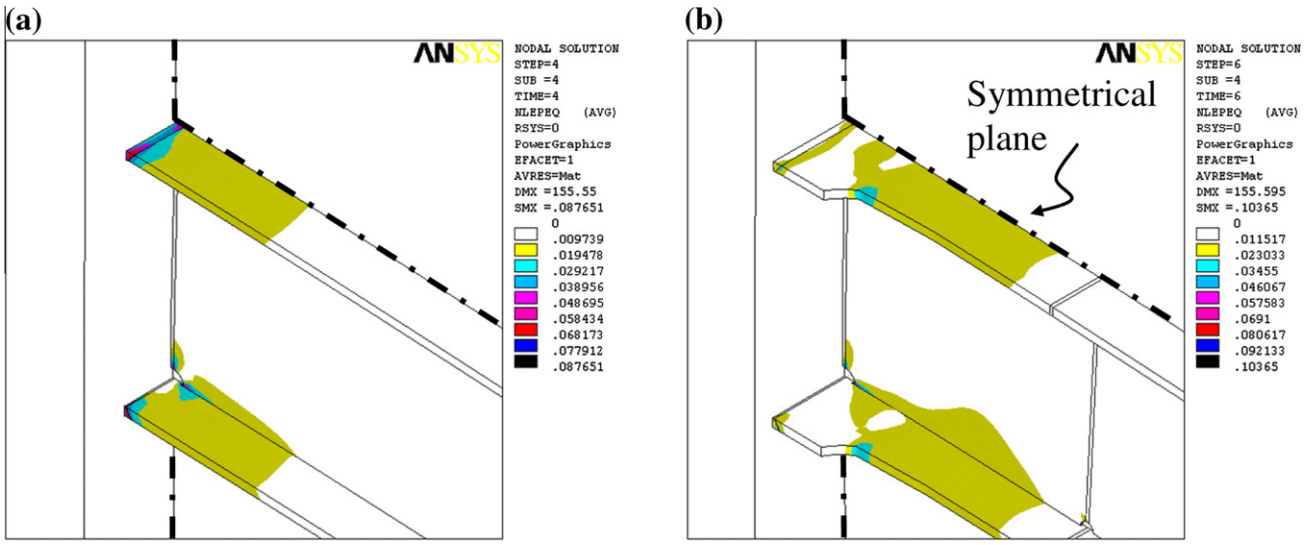

Fig. 21. Contour plots of plastic equivalent strain at 4% rad story drift angle: (a) unreinforced connection; (b) tapered beam flange connection.

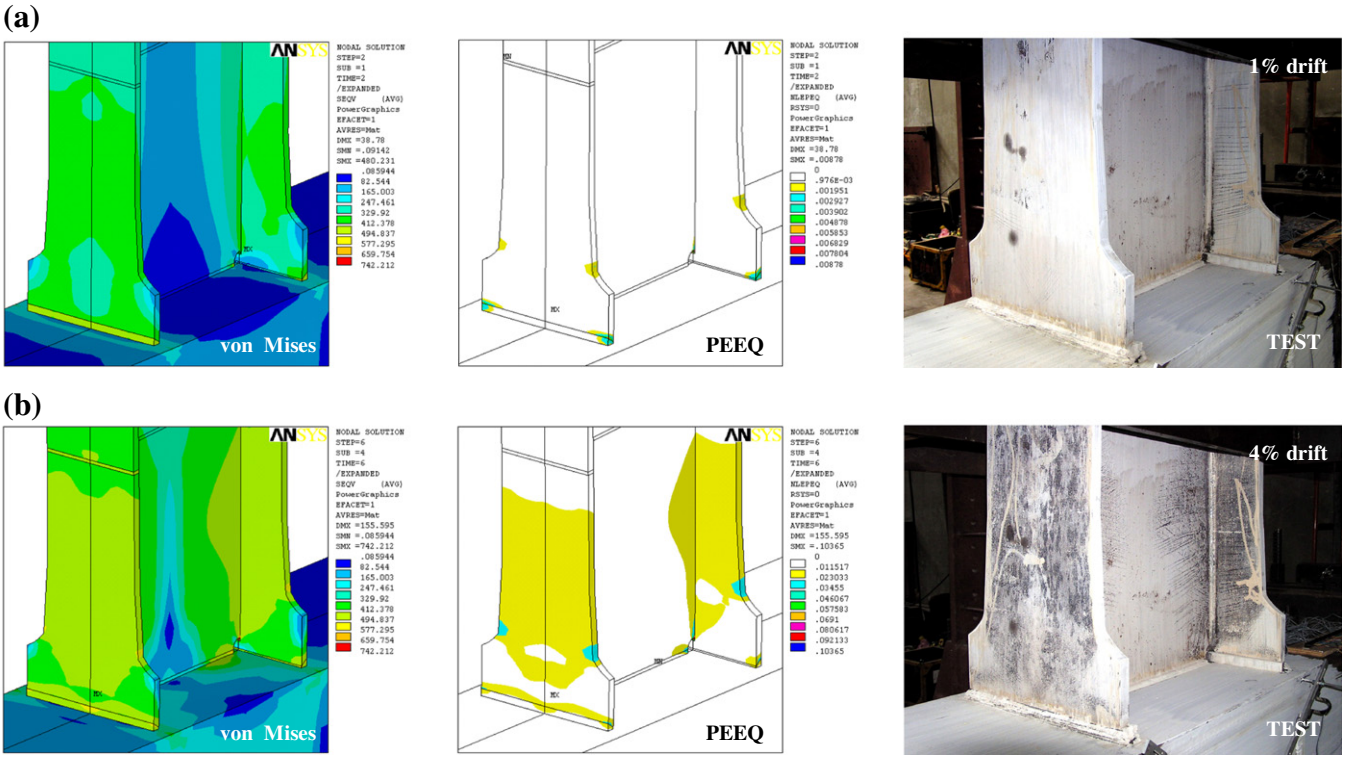

Fig. 22. von Mises stress contours, equivalent plastic strain contours, and yielding behavior during testing of specimen W1-L03: (a) at 1% rad story drift angle and (b) at 4% rad story drift angle.

connection model proceeded to the inelastic range of 4% rad story drift, 62.5% and 42.4% reduction of the maximum PEEQ indices at the edges of the groove weld and at the root of WAH were obtained, respectively, over that of the unreinforced connection model. Certainly, the main reinforced part markedly reduced the high concentration of plastic strain at the beam-to-column joint and the WAH region, ultimately diminishing the potential fracturing at these locations.

4.3.4. Effects of reinforcement ratio β_j and tapered zone length L_{tap}

Exactly how the reinforcement affects the response of the connection subassemblage was investigated by studying four values of reinforcement ratio β_j. Based on engineering practice, the reinforcement ratios were set equal to 1.05, 1.10, 1.20 and 1.25, with the width of the main reinforced part in the range of 344–530 mm. Additionally, exactly how the tapered zone length influences the connection performance was examined through means

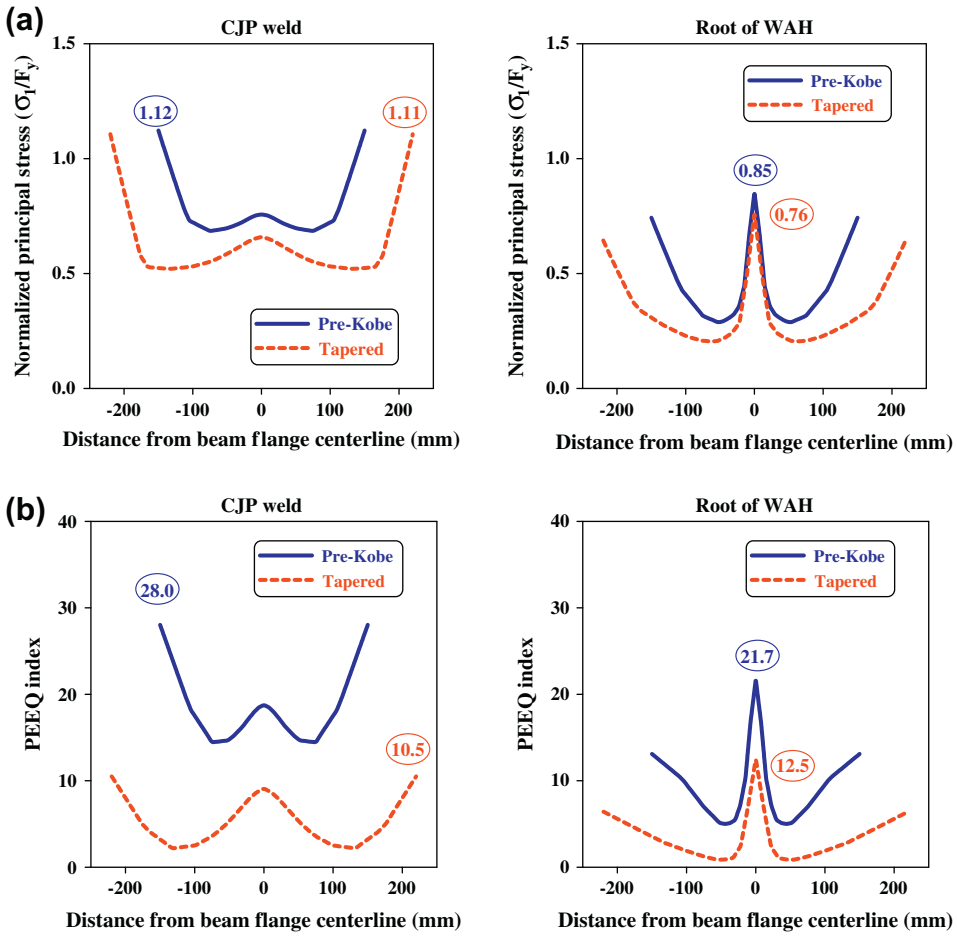

Fig. 23. Distributions of normalized principal stresses and PEEQ indices along beam flange width at the CJP weld and root of WAH: (a) normalized principal stresses at 0.5% rad story drift angle and (b) PEEQ indices at 4% rad story drift angle.

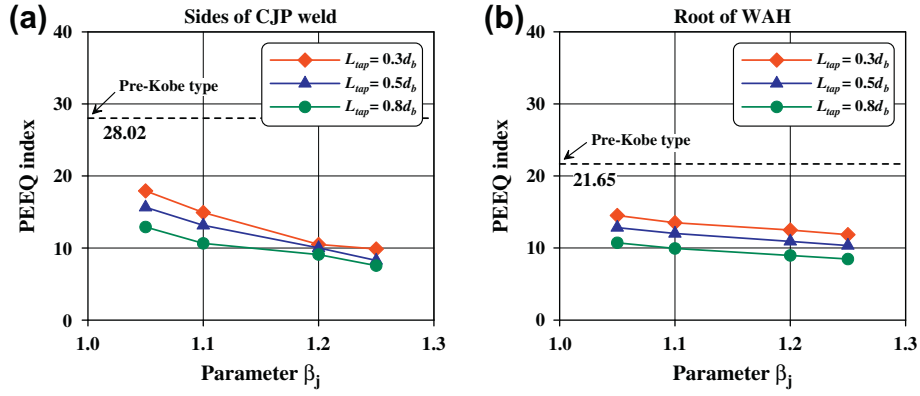

Fig. 24. Effect of parameters of reinforcement ratioβ_j and tapered zone length L_{tap} on PEEQ indices at 4% rad story drift angle: (a) at the CJP weld and (b) at root of WAH.

of varying design parameter L_{tap} by changing the tapered zone length from $0.3d_b$ to $0.8d_b$, ranging from 210 to 560 mm. Fig. 24 summarizes the finite element analysis results. Undoubtedly, the PEEQ indices of the connections were reduced by using the tapered beam flange. The higher reinforcement ratio caused a lower plastic strain demand, resulting in a higher margin of safety at the junction of the beam-to-column connection. Furthermore, using the larger tapered zone also lowered the PEEQ index. According to Fig. 24, the model with reinforcement ratio β_j of 1.05 developed the largest value of PEEQ index at the CJP groove weld that implies the brittle fracture of the beam flange of specimen W3-L03. Based on experimental results and for practical implications, the value of reinforcement ratio β_j can be set to 1.1 or higher and the tapered zone length of $0.3d_b$ can be used.

5. Design considerations

To simplify the design, the thicknesses of the beam flange and web, and beam depth of the tapered beam flange connection are

intentionally assumed to be the same as those of the beam. Based on the parametric study and experimental results, the design parameters of $L_{w1} = 0.5b_f$, $L_{w2} = 50$ mm, and $L_{tap} = 0.3d_b$ can be used in practice. The design procedure to configure the tapered beam flange is summarized as follows.

First, the expected plastic moment of the beam, M_{pe}, is calculated:

$$M_{pe} = R_y F_y Z_b \tag{2}$$

where $R_y F_y$ denotes the expected yield strength; R_y is the ratio of the expected yield strength to the specified minimum yield strength, in accordance with AISC seismic provisions [19]; and Z_b represents the plastic section modulus of the beam.

Second, the maximum width of the tapered beam flange, $b_{f,tap}$, is determined by calculating the design flexural capacity at this location, $M_{p,tap}$, which can be determined based on the moment gradient diagram shown in Fig. 3.

$$M_{p,tap} = \frac{L_b - (L_{w1} + L_{w2})}{L_b - (L_{w1} + L_{w2} + L_{tap})} M_{pe} \tag{3}$$

where L_b refers to the length of the half clear span of the beam.

Third, the width of the main reinforced part, b_{fj}, is designed based on the design flexural capacity at the beam-to-column joint, $M_{p,j}$, which can be determined as

$$M_{p,j} = \beta_j M_{dem,j} \tag{4}$$

where $M_{dem,j}$ denotes the moment demand of the beam at the beam-to-column joint, and can be calculated as

$$M_{dem,j} = \frac{L_b}{L_b - (L_{w1} + L_{w2} + L_{tap})} M_{pe} \tag{5}$$

According to test results, parameter β_j can be set to 1.1 or greater to prevent failure at the beam flange groove weld and the WAH region.

Additionally, the shear demand of the bolted web connection at the beam-to-column joint, $V_{dem,j}$, must be determined to ensure sufficient capacity at this critical section. Design shear for the shear tab and bolts can be calculated as

$$V_{dem,j} = \frac{M_{dem,j}}{L_b} + V_g \tag{6}$$

where V_g is the shear at the column face due to factored gravity loads.

Moreover, a smooth force transfer can be made using the radius of the curved part $R = L_{w1}$. Additionally, the extension length, L_{ext}, can be selected at least $0.5d_b$ to provide a sufficient margin of safety at the splice. Moreover, because the tapered beam flange increases the flexural strength of the beam, the seismic design requirements for a strong-column weak-beam criterion should be checked for designing the tapered beam flange connection.

6. Conclusions

Based on experimental and finite element analysis results for unreinforced pre-Kobe connection and tapered beam flange connections, we conclude the following:

1. While occurring at either the tips of the beam flange groove welds or the root of the weld access hole region, concentrated principal stresses and plastic equivalent strains were noticed in the unreinforced pre-Kobe connection. This appearance of the localized stress and strain resulted in the crack initiation and subsequent beam flange fracture.
2. The tapered beam flange can develop an extensive plastification spread around the tapered zone of the beam away from the column face, in addition to diminishing the stress concentration and plastic strain demand in the beam groove weld and the weld access hole region by using the main reinforced part.
3. Test results of the unreinforced pre-Kobe connection specimen revealed moderate ductile behavior of 2.6% rad plastic rotation. However, the specimen still failed in brittle beam flange fracture at a story drift angle of 4% rad due to cracks initiated at tips of the beam groove weld and in the toe of the weld access hole.
4. Experimental results demonstrated that all tapered beam flange specimens, with either column-tree connection (Series W) or pre-Northridge web-bolted flange-welded connection (Series B), can develop a sufficient rotation of story drift angle, satisfying the requirements for connections used in special moment frames.
5. The parametric study indicated that the behavior of a tapered beam flange connection is influenced mainly by the reinforcement ratio at the beam-to-column joint and the tapered zone length. A larger reinforcement ratio increases the capacity at the CJP groove welds, resulting in a higher margin of safety at the beam-to-column joint. The longer tapered zone of the beam flange leads to a lower plastic strain demand at the CJP groove welds and the weld access hole region.

Acknowledgement

The authors would like to thank the National Science Council of the Republic of China, Taiwan, for financially supporting this research.

References

[1] Tremblay R, Timler P, Bruneau M, Filiatrault A. Performance of steel structures during the 1994 Northridge earthquake. Can J Civil Eng 1995;22:338–60.
[2] Miller DK. Lessons learned from the Northridge earthquake. Eng Struct 1998;20(4–6):249–60.
[3] Mahin ST. Lessons from damage to steel buildings during the Northridge earthquake. Eng Struct 1998;20(4–6):261–70.
[4] Engelhardt MD, Winneberger T, Zekany AJ, Potyraj TJ. Experimental investigation of dogbone moment connections. Eng J AISC 1998;35(4):128–39.
[5] Uang CM, Bondad D, Lee CH. Cyclic performance of haunch repaired steel moment connections: experimental testing and analytical modeling. Eng Struct 1998;20(4–6):552–61.
[6] Engelhardt MD, Sabol TA. Reinforcing of steel moment connections with cover plates: benefits and limitations. Eng Struct 1998;20(4–6):510–20.
[7] Azuma K, Kurobane Y, Makino Y. Cyclic testing of beam-to-column connections with weld defects and assessment of safety of numerically modeled connections from brittle fracture. Eng Struct 2000;22:1596–608.
[8] Lu LW, Ricles JM, Mao C, Fisher JW. Critical issues in achieving ductile behaviour of welded moment connections. J Constr Steel Res 2000;55(1–3):325–41.
[9] FEMA-350. Recommended seismic design criteria for new steel moment-frame buildings. Washington (DC): Federal Emergency Management Agency; 2000.
[10] ANSI/AISC 358. Prequalified connections for special and intermediate steel moment frames for seismic applications. Chicago (IL): American Institute of Steel Construction, Inc.; 2005.
[11] SAC Joint Venture. Interim guidelines: evaluation, repair, modification and design of steel moment frames, report no. SAC-95-02. Sacramento, CA: SAC Joint Venture; 1995.
[12] Nakashima M, Suita K, Morisako K, Maruoka Y. Tests of welded beam–column subassemblies, I: Global behavior. J Struct Eng, ASCE 1998;124(11):1236–44.
[13] McMullin KM, Astaneh-Asl A. Steel semirigid column-tree moment resisting frame seismic behavior. J Struct Eng, ASCE 2003;129(9):1243–9.
[14] Nakashima M, Inoue K, Tada M. Classification of damage to steel buildings observed in the 1995 Hyogoken-Nanbu earthquake. Eng Struct 1998;20(4–6):271–81.
[15] Zepeda JA, Itani AM, Sahai R. Cyclic behavior of steel moment frame connections under varying axial load and lateral displacements. J Constr Steel Res 2003;59:1–25.
[16] Sugimoto H, Morita K, Takahashi Y. Prediction of failure mode of hunched beam to SHS column connections. Int J Steel Struct 2001;1(3):185–99.
[17] Roeder CW. General issues influencing connection performance. J Struct Eng ASCE 2002;128(4):420–8.
[18] Chen CC, Lin CC, Tsai CL. Evaluation of reinforced connections between steel beams and box columns. Eng Struct 2004;26(13):1889–904.

[19] American Institute of Steel Construction (AISC). Seismic provisions for structural steel buildings. Chicago (IL): American Institute of Steel Construction, Inc.; 2005.
[20] Chen CC, Chen SW, Chung MD, Lin MC. Cyclic behaviour of unreinforced and rib-reinforced moment connections. J Constr Steel Res 2005;61(1):1–21.
[21] ANSYS user manual. Swanson Analysis Systems, Inc.; 2002.
[22] Popov EP, Yang TS, Chang SP. Design of steel MRF connections before and after 1994 Northridge earthquake. Eng Struct 1998;20(12):1030–8.
[23] El-Tawil S, Mikesell T, Kunnath SK. Effect of local details and yield ratio on behavior of FR steel connections. J Struct Eng ASCE 2000;126(1):79–87.
[24] Mao C, Ricles J, Lu LW, Fisher J. Effect of local details on ductility of welded moment connections. J Struct Eng, ASCE 2001;127(9):1036–44.
[25] Chen CC, Lu CA, Lin CC. Parametric study and design of rib-reinforced steel moment connections. Eng Struct 2005;27(5):699–708.
[26] Stojadinović B, Goel SC, Lee KH, Margarian AG, Choi JH. Parametric tests on unreinforced steel moment connections. J Struct Eng, ASCE 2000;126(1):40–9.
[27] Kim T, Stojadinovic B, Whittaker AS. Seismic performance of US steel box column connections. In: Proc 13th world conference on earthquake eng. Canada; 2004 [paper no. 981].